IEEE Photonics Journal
An IEEE Photonics Society Publication

Open Access

Tunable Plasmonic Wavelength Demultiplexing Device Using Coupled Resonator System

Volume 8, Number 3, June 2016

Xiao-Meng Geng
Tie-Jun Wang
Da-Quan Yang
Lin-Yan He
Chuan Wang

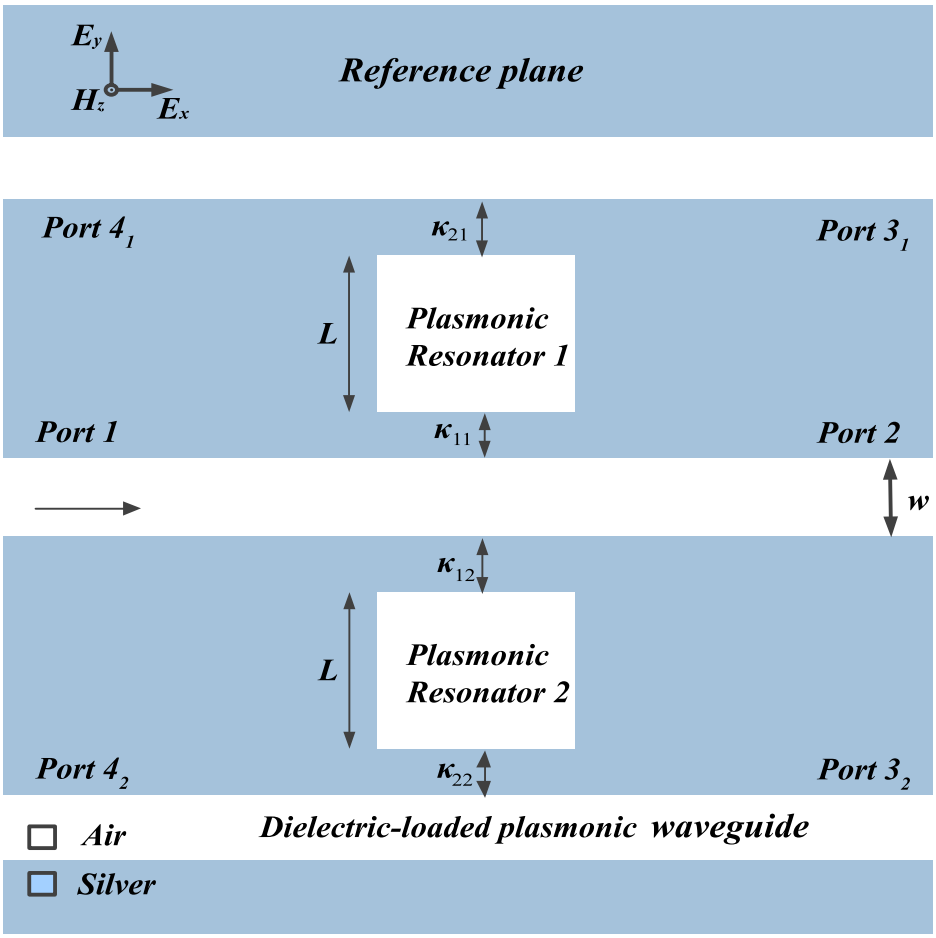

DOI: 10.1109/JPHOT.2016.2573041
1943-0655

Tunable Plasmonic Wavelength Demultiplexing Device Using Coupled Resonator System

Xiao-Meng Geng,[1,2] Tie-Jun Wang,[1,2] Da-Quan Yang,[1,3] Lin-Yan He,[1,2] and Chuan Wang[1,2]

[1]State Key Laboratory of Information Photonics and Optical Communications, Beijing University of Posts and Telecommunications, Beijing 100876, China
[2]School of Science, Beijing University of Posts and Telecommunications, Beijing 100876, China
[3]School of Information and Communication Engineering, Beijing University of Posts and Telecommunications, Beijing 100876, China

DOI: 10.1109/JPHOT.2016.2573041

Manuscript received May 3, 2016; accepted May 18, 2016. Date of publication May 25, 2016; date of current version June 16, 2016. This work was supported in part by the National Natural Science Foundation of China under Grant 61471050, Grant 11404031, and Grant 61501053 and in part by the Fund of State Key Laboratory of Information Photonics and Optical Communications (Beijing University of Posts and Telecommunications). Corresponding author: C. Wang (e-mail: wangchuan@bupt.edu.cn).

Abstract: Plasmonic devices have recently been widely studied recently due to their properties of light confinement, which shows great potential applications in optical information processing. Here, in exploiting plasmonic metal–insulator–metal (MIM) side-coupled cavities, we present a theoretical implementation of the plasmonic wavelength demultiplexer (PWDM) device. The proposed PWDM device is designed using an add–drop-drop structure, which consists of one input port and two output ports. The transmission of the plasmonic field on the drop ports could be tuned by changing the gap between the waveguide and plasmonic resonators. Our approach captures the wavelength demultiplexing properties of the plasmonic field using the proposed structure. The performance of our device is analyzed based on the structure with three waveguides coupled with two square cavities.

Index Terms: Plasmonic wavelength demultiplexer, add–drop, tunable.

1. Introduction

Exploiting surface plasmons (SPs), which are the coherent delocalized electron oscillations that exist at the interface between any two materials, various plasmonic devices can be realized, which overcomes the size limitations of photonic circuits, and further used in high performance data processing and quantum information science [1], [2]. Over the past few decades, various implementations of plasmonic devices have been demonstrated, such as plasmonic switches [3], couplers [4], modulators [5], photovoltaics devices [6], and so on. Among these plasmonic devices, metal-insulator-metal (MIM) waveguides are promising candidates for the realization of nanoscale devices. For example, various applications of MIM waveguides have been investigated using MIM waveguides, such as demultiplexers [7] and filters [8], [9].

Among these configurations, the structure based on plasmonic resonators is widely studied for novel nanophotonic devices, especially in multiplexers and optical switches. By combining two waveguides side coupled with the resonator, the add-drop plasmonic structure can be implemented. Recently, add-drop devices have been implied in all-fiber architectures [10], photonic

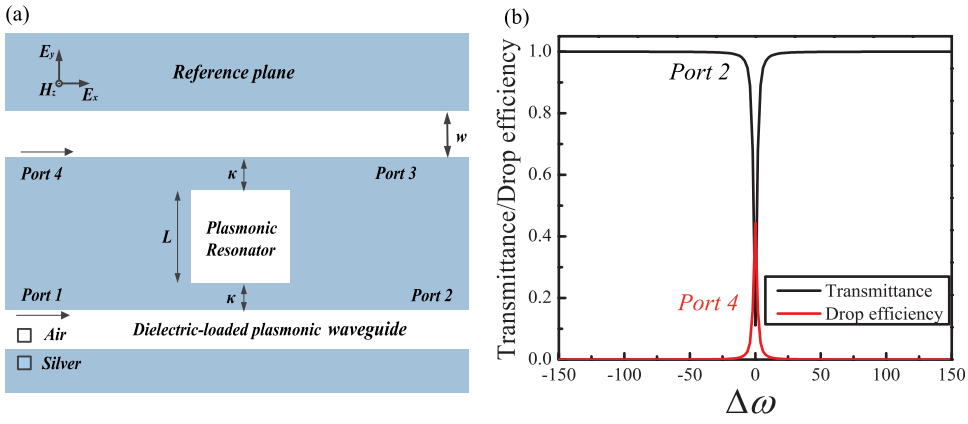

Fig. 1. (a) Schematic of the add–drop waveguides coupled with a square cavity. The SPs is injected from the port 1 (input port) of a bus waveguide and will be transferred to the port 4 (drop port) and port 2 (throughput port). Furthermore, the coupling gaps are defined as *g*. In this illustration, the port 3 (add port) is left at vacuum ($a_3 = 0$). (b) Theoretical transmission and drop efficiency of the structure, as shown in (a). The spectra are calculated from (3) and (4) with $\kappa_0 = \kappa_1 = \kappa_2$.

crystals [11], [12], and whispering-gallery-mode microcavities [13]. The proposed structure provides large off-off-band signal rejection [14]. For example, Vörckel *et al.* reported an asymmetrical coupling of the signal waveguides to the resonator, and attained a higher throughput attenuation and drop efficiency [15]. Monifi *et al.* demonstrated an add-drop structure optical filter using microtoroid resonators [16]. Moreover, it has wide applications ranging from magneto-optic data storage [17], construct sensors [18], [19], and modulators [20] to biological detection [21] since it was proposed. As the plasmonic device is the main solution of integrate photonic circuit which can overcome the diffraction limit and has the applications in nanoscale devices, it has gradually become the hot spot of research; for example, Liu *et al.* [22] first introduced a compact plasmonic add-drop coupler with square ring resonator and further proposed L-shaped and T-shaped bends. This new structure could achieve flexible flow control at waveguide junctions and exhibits the potential to be used in high density photonic circuits.

Motivated by the implementation of nanophotonic device based on add-drop structure, we proposed the plasmonic wavelength demultiplexer (PWDM) that based on the strongly-confined MIM plasmonic waveguides. In this paper, we investigate a compact structure of an add-drop-drop device using the MIM waveguide-resonator system. The proposed system consists of three MIM waveguides coupled with two square resonators. The theoretical results show the difference of transmission field on different drop ports. The numerical simulation reveals the relationship between the length of the square cavity and the transmittance or the reflection of the plasmonic field, which shows good agreement with the theoretical results. The spectra features could be utilized to achieve wavelength demultiplexers.

2. The Model of Add-Drop Plasmonic Waveguide-Resonators Coupled System

Considering the case of radiative resonator in MIM waveguides, a compact add-drop structure model is shown in Fig. 1(a).The bus waveguide and the drop waveguide with the same width *w* are coupled with the square resonator (length L). The distance between the bus waveguide (add-drop waveguide) and the rectangle resonator are set as *g* and defines the coupling loss as κ. Therefore, when *g* is small enough, the transverse-magnetic (TM) wave will be existed in this square cavity because of near-field coupling. In other words, SPs waves are generated on the metal-insulator interfaces on port 1. And when the SPs pass through the bus waveguide, waves could couple into the square resonator, and pass through the throughput port and drop port. Here, we choose the materials in the structure as silver (ε_m) and air ($\varepsilon = 1$), shown the blue

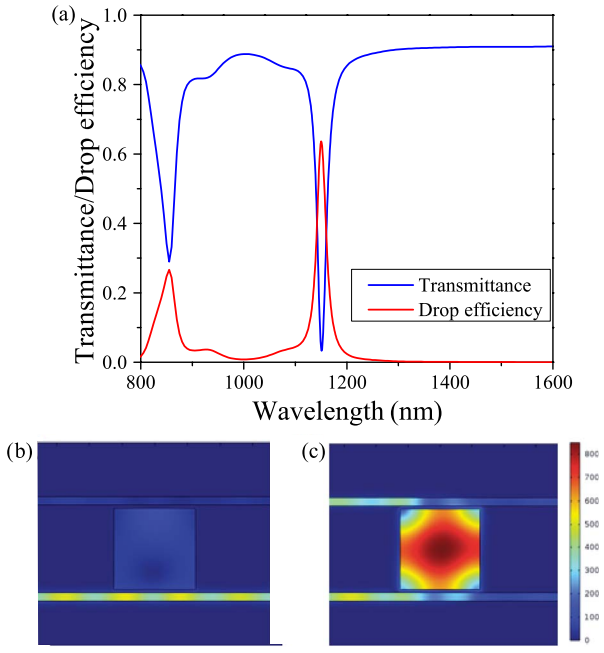

Fig. 2. (a) Transmission spectra of the structure with a square cavity with $L = 500$ nm, $w = 50$ nm, and $g = 20$ nm, and the dips appear at the 855 and 1150 nm; and electric field distribution of SPs at the resonant wavelengths (b) 1000 nm and (c) 1150 nm.

and white areas in Fig.1(a). The frequency-dependent complex relative permittivity of silver [23] is determined by the Drude model

$$\varepsilon_m = \varepsilon_\infty - \frac{\omega_p^2}{\omega(\omega + i\gamma)} \tag{1}$$

where $\varepsilon_\infty = 3.7$ is the dielectric constant at infinite angular frequency, $\omega_p = 9.1$ eV is the bulk plasma frequency, $\gamma = 0.018$ eV denotes the damping frequency, and ω represents for the angular frequency of the incident electromagnetic radiation.

Here, we investigate the theoretical model of the system by using coupled-mode theory [24]. Denoting the resonator total intrinsic loss, the bus-resonator coupling loss, and the drop-resonator coupling loss as κ_0, κ_1, and κ_2, respectively, the field amplitude of SPs in the resonator could be described as

$$\frac{da}{dt} = j\omega_0 a - \left(\frac{\kappa_0 + \kappa_1 + \kappa_2}{2}\right) a + \sqrt{\kappa_1} a_1 \tag{2}$$

where a represents the amplitude of the intracavity field, ω_0 is the central resonance frequency of the cavity, and a_i $(i = 1, 2, 3, 4)$ denotes the incoming and outgoing waves, respectively. The input-output relations for the add port (port 2) and drop port (port 4) can be described by $a_2 = a_1 - \sqrt{\kappa_1} a$, and $a_4 = a_3 - \sqrt{\kappa_2} a$. In our case, only the input port from port 1 is employed and there is no input at the port 3, that is to say $a_3 = 0$. The transmission (T) and drop efficiency (D) could be solved in a steady state as

$$T = \left|\frac{a_2}{a_1}\right|^2 = \frac{4\Delta^2 + (\kappa_0 - \kappa_1 + \kappa_2)^2}{4\Delta^2 + (\kappa_0 + \kappa_1 + \kappa_2)^2} \tag{3}$$

$$D = \left|\frac{a_4}{a_1}\right|^2 = \frac{4\kappa_1\kappa_2}{4\Delta^2 + (\kappa_0 + \kappa_1 + \kappa_2)^2}. \tag{4}$$

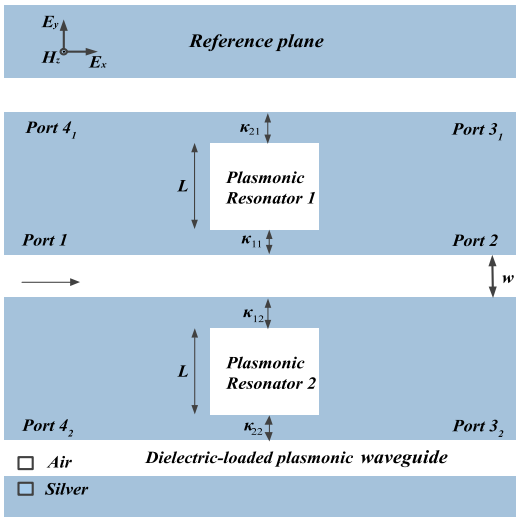

Fig. 3. Schematic of the three waveguides coupled with two different square cavities. The bus waveguide and the add–drop-drop waveguide with the same width w are coupled with the two square resonators (length L), respectively. The cavity decay rates are denoted by κ_{01} and κ_{02}, respectively.

For simplicity, we assumed that $\kappa_0 = \kappa_1 = \kappa_2$ and the transmission and the drop efficiency are plotted in Fig. 1(b). It could be observed that the dip of the transmission spectra appears, and the drop efficiency spectra peak is also appeared in the same position. Next we simulate this structure by the finite-difference time-domain (FDTD) method, here the parameters are set to be as $L = 500$ nm, $w = 50$ nm, the distance between the waveguide and the resonator is $g = 20$ nm. As shown in Fig. 2(a), two resonance dips appear in the transmission spectra at 885 nm and 1150 nm, respectively. And the distributions of the electric field density are shown in Fig. 2(b) and (c), the SPs pass through from port 4 when it reaches the resonant wavelength of 1150 nm, and little SPs waves pass through from port 2. However, the waves around 1000 nm could transmit the structure through port 2 without reflection from port 4.

3. The Implementation of PWDM Using Add-Drop-Drop Structure Plasmonic Waveguide-Resonator System

In the previous works, the add-drop structure could be investigated as the filters in optical communication systems. Here, we generalized the add-drop structure to the add-drop-drop structure in the MIM plasmonic waveguides and the schematic structure is shown in Fig. 3. The proposed structure consists of three waveguides coupled with two square cavities (marked with resonator 1 and resonator 2) with different lengths. The bus waveguide and the add-drop-drop waveguide with the same width w are coupled with the two square resonators (length L), respectively. The cavity decay rates are denoted by κ_{01} and κ_{02}, respectively, and the coupling decay rate between the waveguides and the resonators are represented by κ_{11}, κ_{12}, κ_{21}, and κ_{22}. Then, we can write the equations of the fields as follows:

$$\frac{da_i}{dt} = j\omega a_i - \frac{\kappa_{0i} + \kappa_{1i} + \kappa_{2i}}{2} a + \sqrt{\kappa_{1i}} a_{\text{in}} \tag{5}$$

and the input-output relation under the steady state solution could be described as

$$a_2 = a_{\text{in}} - (\sqrt{\kappa_{11}} a_1 + \sqrt{\kappa_{21}} a_2) \tag{6}$$

$$a_{4i} = \sqrt{\kappa_{2i}} a_i \tag{7}$$

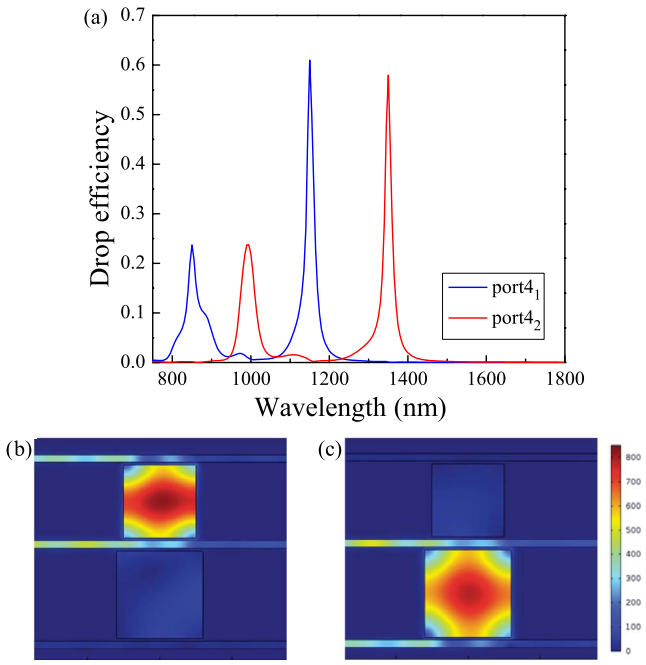

Fig. 4. (a) Transmission spectrum of the three waveguides coupled with two cavities under $L_1 = 500$ nm, $L_2 = 600$ nm, $\omega = 50$ nm, and $g = 20$ nm. The blue line is corresponding to the drop efficiency of the port 4_1, and the red line is corresponding to the drop efficiency of the port 4_2. Electric field distribution of SPs at the resonant wavelengths (b) 1150 and (c) 1350 nm. In addition, we can also find that the port $4_1$1 have a broaden full-width-half maximum (FWHM) than port 4_2 because of the cavity 2 has a larger intrinsic loss under the same coupling distances.

where $i = 1, 2$. According to the input-output relations, the transmission efficiencies at the drop ports can be solved as

$$D_{41} = \left|\frac{a_{41}}{a_{\text{in}}}\right|^2 = \frac{4\kappa_{11}\kappa_{21}(\kappa_{01}+\kappa_{11}+\kappa_{21})^2 + 16\kappa_{11}\kappa_{21}\Delta^2}{4\Delta^2 + (\kappa_{01}+\kappa_{11}+\kappa_{21})^2}, \tag{8}$$

$$D_{42} = \left|\frac{a_{42}}{a_{\text{in}}}\right|^2 = \frac{4\kappa_{12}\kappa_{22}(\kappa_{02}+\kappa_{12}+\kappa_{22})^2 + 16\kappa_{12}\kappa_{22}\Delta^2}{4\Delta^2 + (\kappa_{02}+\kappa_{12}+\kappa_{22})^2}, \tag{9}$$

where D_{41} and D_{42} represent the transmission coefficients of the drop ports 4_1 and port 4_2. To investigate the transmission properties of the plasmonic circuit, we numerically studied the field distribution and resonance of the field by varying the scale of the cavities. Here in Fig. 4(a), the peak wavelength under the width $(\omega = 50\ \text{nm})$ of bus waveguides and with the gap width (20 nm) is presented, and the transmitted field with different wavelength (1150 nm and 1350 nm) could be observed at different ports as shown in Fig. 4(b) and (c).

According to the previous simulation, we find that the proposed system exhibits potential applications for PWDM. Here we set port 1 as the input port, and the parameters of the structure are set to be $L_1 = 500$ nm, $L_2 = 600$ nm, $\omega = 50$ nm, and $\kappa_{11} = \kappa_{12} = \kappa_{21} = \kappa_{22}$. As shown in Fig. 4(a), we can see that the wavelength of 1150 nm and 1350 nm can be separated, and the reflectivity approaches 64%. Moreover, we further studied the transmission properties of the circuit by varying the scale and the coupling strength of the cavity. Here, in Fig. 5(a), we only focus on the field distribution at the drop port by changing the scale of the resonator from 500 nm to 700 nm and simulated the resonant frequency of two modes from 800 nm to 1800 nm. The resonant wavelength exhibits the red shifts behavior, and the drop efficiency decreases with the increment of the cavity length. Moreover in Fig. 5(b), the reflectivity of the spectrum decreases

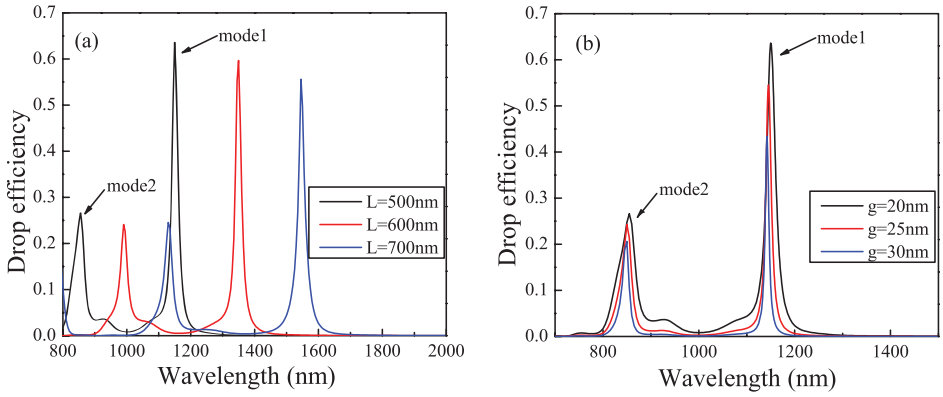

Fig. 5. Transmission at the drop port for different cavities. Here, the black, red, and blue lines are the transmission spectrum at the cavity length with L = 500 nm, $L = 600$ nm, and $L = 700$ nm, respectively.

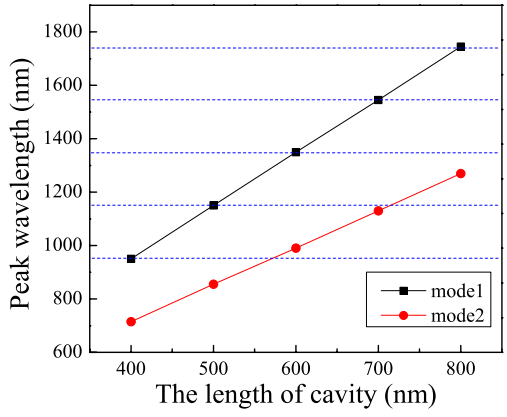

Fig. 6. Relation between the transmission peak wavelength and the length of the cavity. Crosstalk will happen only when $L_1 = 400$ nm ($L_2 = 600$ nm) and $L_1 = 500$ nm ($L_2 = 700$ nm). However, our structure has a narrow FWHM, and the slopes factor of the line of mode 1 is more than mode 2; thus, the crosstalk will not occur again.

with the gap width increment, and it also reveals that the coupling strength increases with the decrement of the gap width. This structure can get a narrowband wavelength selection by choosing suitable gap width and the length of cavity. We all know that it has three wavelengths in fiber optic communications, and these wavelengths are 850 nm, 1310 nm, and 1550 nm, respectively. While these wavelengths are well conformed to our resonance wavelengths, that is to say our structure will have a promising function. Here in Fig. 6, the relation between the transmission peak wavelength and the length of the cavity is shown. The black and red lines represent the two different modes of the transmission spectrum. It is obvious that the transmitted frequency becomes red shift along with the increment of the cavity length. Here, the blue dashed lines are added in Fig. 6. We can conclude that the crosstalk only occurs when $L_1 = 400$ nm ($L_2 = 600$ nm) and $L_1 = 500$ nm ($L_2 = 700$ nm). However, as our structure exhibits a narrow FWHM and the slopes factor of the line of mode 1 is more than mode 2, therefore, the crosstalk will not occur again.

4. Summary

In summary, we investigated an implementation of PWDM device based on plasmonic MIM waveguides coupled with two rectangle cavities. The transmission properties of the structure

are theoretically analyzed. We found that the transmission of plasmonic field on the drop ports could be tuned by changing the gap between the waveguide and plasmonic resonators, as well as the size of the cavity. The proposed structure is suitable for demultiplexing of the plasmonic wideband signals. The dependences of demultiplexed wavelength of each channel on geometrical parameters of the structure are discussed. The wavelength demultiplexing structure might become a choice for the design of all-optical integrated architectures for optical computing and optical communication. As 850 nm, 1310 nm and 1550 nm are commercial used wavelengths in fiber optic communications, our scheme provides a potential practical application in all-optical communication system with these wavelengths are well conformed to our resonance wavelengths. Recently, we noticed that Hu *et al.* [25] also introduced a wavelength demultiplexing structure based on arrayed plasmonic slot cavities. Compared with our scheme, they provide more channels to achieve more wavelengths demuliplexing, but our structure has a nearly 20% intensity of the drop efficiency above the 1000 nm and exhibits a bigger coupling distance than the arrayed plasmonic slot cavities; therefore, we can say that our structure will be easily achieved in experiments.

References

[1] E. Ozbay, "Plasmonics: Merging photonics and electronics at nanoscale dimensions," *Science*, vol. 311, no. 5758, pp. 189–193, 2006.

[2] D. K. Gramotnev and S. I. Bozhevolnyi, "Plasmonics beyond the diffraction limit," *Nature Photon.*, vol. 4, no. 2, pp. 83–91, 2010.

[3] R. A. Pala, K. T. Shimizu, and N. A. Melosh, "A nonvolatile plasmonic switch employing photochromic molecules," *Nano Lett.*, vol. 8, no. 5, pp. 1506–1510, May 2008.

[4] G. Veronis and S. Fan, "Theoretical investigation of compact couplers between dielectric slab waveguides and two-dimensional metal-dielectric-metal plasmonic waveguides," *Opt. Exp.*, vol. 15, no. 3, pp. 1211–1221, 2007.

[5] J. A. Dionne, K. Diest, and L. A. Sweatlock, "PlasMOStor: A metal-oxide-Si field effect plasmonic modulator," *Nano Lett.*, vol. 9, no. 2, pp. 897–902, Feb. 2009.

[6] H. A. Atwater and A. Polman, "Plasmonics for improved photovoltaic devices," *Nature Mater.*, vol. 9, no. 3, pp. 205–213, Mar. 2010.

[7] X. Mei, X. Huang, J. Tao, J. Zhu, Y. Zhu, and X. Jin, "A wavelength demultiplexing structure based on plasmonic MDM side-coupled cavities," *J. Soc. Amer. B*, vol. 27, no. 12, pp. 2707–2713, 2010.

[8] A. Hosseini, H. Nejati, and Y. Massoud, "Design of a maximally flat optical low pass filter using plasmonic nanostrip waveguides," *Opt. Exp.*, vol. 15, no. 23, pp. 15280–15286, Nov. 2007.

[9] Y. Guo *et al.,* "Characteristics of plasmonic filters with a notch located along rectangular resonators," *Plasmonics*, vol. 8, pp. 167–171, 2013.

[10] F. Bilodeau *et al.*, "An all-fiber dense-wavelength-division multiplexer/demultiplexer using photoimprimed Bragg gratings," *IEEE Photon. Technol. Lett.*, vol. 7, no. 4, pp. 388–390, Apr. 1995.

[11] Z. Qiang, W. Zhou, and R. A. Soref, "Optical add-drop filters based on photonic crystal ring resonators," *Opt. Exp.*, vol. 15, no. 4, pp. 1823–1831, Feb. 2007.

[12] K. Tao, J.-J. Xiao, and X. Yin, "Nonreciprocal photonic crystal add-drop filter," *Appl. Phys. Lett.*, vol. 105, 2014, Art. no. 211105.

[13] F. Monifi, J. Friedlein, Ş. K. Özdemir, and L. Yang, "A robust and tunable add-drop filter using whispering gallery mode microtoroid resonator," *J. Lightw. Technol.*, vol. 30, no. 21, pp. 3306–3315, Nov. 2012.

[14] B. Little, S. Chu, H. Haus, J. Foresi, and J.-P. Laine, "Microring resonator channel dropping filters," *J. Lightw. Technol.*, vol. 15, no. 6, pp. 998–1005, Jun. 1997.

[15] A. Vörckel, M. Mönster, W. Henschel, P. H. Bolivar, and H. Kurz, "Asymmetrically coupled silicon-on-insulator microring resonators for compact add-drop multiplexers," *IEEE Photon. Technol. Lett.*, vol. 15, no. 7, pp. 921–923, Jul. 2003.

[16] F. Monifi, S. K. Özdemir, and L. Yang, "Tunable add-drop filter using an active whispering gallery mode microcavity," *Appl. Phys. Lett.*, vol. 103, no. 18, 2013, Art. no. 181103.

[17] M. Mansuripur *et al.,* "Plasmonic nano-structures for optical data storage," *Opt. Exp.*, vol. 17, no. 16, pp. 14001–14014, Aug. 2009.

[18] G. Nemova and R. Kashyap, "Theoretical model of a planar waveguide refractive index sensor assisted by a corrugated long period metal grating," *Opt. Commun.*, vol. 281, no. 6, pp. 1522–1528, Mar. 2008.

[19] S. Enoch, R. Quidant, and G. Badenes, "Optical sensing based on plasmon coupling in nanoparticle arrays," *Opt. Exp.*, vol. 12, no. 15, pp. 3422–3427, Jul. 2004.

[20] T. Nikolajsen, K. Leosson, and S. I. Bozhevolnyi, "Surface plasmon polariton based modulators and switches operating at telecom wavelengths," *Appl. Phys. Lett.*, vol. 85, pp. 5833–5835, 2004.

[21] B. Liedberg, C. Nylander, and I. Lunström, "Surface plasmon resonance for gas detection and biosensing," *Sens. Actuators*, vol. 4, pp. 299–304, 1983.

[22] J. Liu, G. Fang, H. Zhao, Y. Zhang, and S. Liu, "Plasmon flow control at gap waveguide junctions using square ring resonators," *J. Phys. D, Appl. Phys.*, vol. 43, no. 5, 2010, Art. no. 055103.

[23] P. B. Johnson and R.-W. Christy, "Optical constants of the noble metals," *Phys. Rev. B*, vol. 6, pp. 4370–4379, 1972.
[24] A. Yariv, "Coupled-mode theory for guided-wave optics," *IEEE J. Quantum Electron.*, vol. 9, no. 9, pp. 919–933, Sep. 1973.
[25] F. Hu, H. Yi, and Z. Zhou, "Wavelength demultiplexing structure based on arrayed plasmonic slot cavities," *Opt. Lett.*, vol. 36, no. 8, pp. 1500–1502, 2011.